

RESEARCH ARTICLE | *Neurogastroenterology and Motility*

Shifting into high gear: how interstitial cells of Cajal change the motility pattern of the developing intestine

 Nicolas R. Chevalier,¹ Yanis Ammouche,¹ Anthony Gomis,¹ Clémence Teysaie,¹ Pascal de Santa Barbara,² and Sandrine Faure²

¹Laboratoire Matière et Systèmes Complexes, Université de Paris/CNRS UMR 7057, Sorbonne Paris Cité, 75013 Paris, France; and ²PhyMedExp, University of Montpellier, INSERM, CNRS, Montpellier, France

Submitted 7 April 2020; accepted in final form 19 August 2020

Chevalier NR, Ammouche Y, Gomis A, Teysaie C, de Santa Barbara P, Faure S. Shifting into high gear: how interstitial cells of Cajal change the motility pattern of the developing intestine. *Am J Physiol Gastrointest Liver Physiol* 319: G519–G528, 2020. First published September 2, 2020; doi:10.1152/ajpgi.00112.2020.—The first contractile waves in the developing embryonic gut are purely myogenic; they only involve smooth muscle. Here, we provide evidence for a transition from smooth muscle to interstitial cell of Cajal (ICC)-driven contractile waves in the developing chicken gut. In situ hybridization staining for anoctamin-1 (ANO1), a known ICC marker, shows that ICCs are already present throughout the gut, as from embryonic day (E)7. We devised a protocol to reveal ICC oscillatory and propagative calcium activity in embryonic gut whole mount and found that the first steady calcium oscillations in ICCs occur on (E14). We show that the activation of ICCs leads to an increase in contractile wave frequency, regularity, directionality, and velocity between E12 and E14. We finally demonstrate that application of the c-KIT antagonist imatinib mesylate in organ culture specifically depletes the ICC network and inhibits the transition to a regular rhythmic wave pattern. We compare our findings to existing results in the mouse and predict that a similar transition should take place in the human fetus between 12 and 14 wk of development. Together, our results point to an abrupt physiological transition from smooth muscle mesenchyme self-initiating waves to ICC-driven motility in the fetus and clarify the contribution of ICCs to the contractile wave pattern.

NEW & NOTEWORTHY We reveal a sharp transition from smooth muscle to interstitial cell of Cajal (ICC)-driven motility in the chicken embryo, leading to higher-frequency, more rhythmic contractile waves. We predict the transition to happen between 12 and 14 embryonic wk in humans. We image for the first time the onset of ICC activity in an embryonic gut by calcium imaging. We show the first KIT and anoctamin-1 (ANO1) in situ hybridization micrographs in the embryonic chicken gut.

calcium imaging; contraction wave; embryo; interstitial cells of Cajal; intestine; motility; pacemaker; smooth muscle

INTRODUCTION

The interstitial cells of Cajal (ICC) are the pacemakers of the intestine (20). They constitute a network of anastomosing cells that present spontaneous, rhythmic oscillations of their membrane potential, called “slow waves” (24, 37). Electrical coupling of these cells to the circular smooth muscle paces the generation of circular contractile waves essential for digestion. They are also electrically connected to the enteric nervous

system (ENS), acting as an intermediate between the ENS and its effector, the smooth muscle (18). ICCs have attracted considerable attention both for their fundamental “clock cell” property (20) and for their potential involvement in conditions like Hirschsprung disease, pyloric stenosis, or chronic intestinal pseudo-obstruction (10).

Both ICCs and smooth muscle originate from the mesoderm (19). ICCs have been detected as early as embryonic day (E) 14.5 in the mouse embryo (30), i.e., at the same time as circular smooth muscle differentiation in the midgut. They reach a mature morphology only around E18.5 in the mouse (30) stage, at which the first slow waves could be recorded by microelectrode impalement (3, 30). Using W/W^v ICC-depleted mutant mice, Roberts et al. (30) concluded that the first circular smooth muscle contractile waves starting at E13.5 are not generated by ICCs. The calcium waves underlying these smooth muscle contractile waves have recently been imaged in the chicken embryo (5, 16). Motility of the adult W/W^v mouse has been further investigated both in vivo (9) and ex vivo (28). All of these studies indicate that smooth muscle alone has the capability to spontaneously generate contractile waves. This myogenic phase precedes any influence of the enteric nervous system on motility because the latter only becomes active later in development [E18.5 in mice (30), E16 in the chicken (6)]. The ICCs are not the only cells that can produce rhythmic motility patterns in the gut: it has recently been shown (31, 32) that the enteric nervous system can also generate rhythmic patterns of coordinated neuronal firing, leading to rhythmic patterns of electrical activity (excitatory and inhibitory junctional potentials) and contractility in the smooth muscle. Adult W/W^v ICC-depleted mutant mice still display exhibit prominent enteric neurogenic activity and cyclical motor complexes still occur (33).

In a recent publication (6), we had measured an abrupt change in the speed of circular smooth muscle contractile waves between E12 and E14 in the chicken intestine, leading us to speculate that a developmental transition to ICC-driven waves could occur around this embryonic stage. The emergence of slow waves in the mouse embryo has been examined by microelectrode single-cell electrophysiological measurements (3, 30, 38). In this report, we strived to measure the effect of ICCs on motility in the embryo by time- and space-resolved techniques: calcium imaging and spatiotemporal contractility maps. Given the lack of information on the development of ICCs in the chicken embryo, we also performed in situ hybridization for the cell surface receptor anoctamin-1

Correspondence: N. R. Chevalier (nicolas.chevalier@univ-paris-diderot.fr).

(ANO1), revealing the ultrastructure of this cell network at early embryonic stages in this important animal model. We compare our results to electrophysiological (3, 30) and motility (9, 28) studies in the mouse, discuss their implications for humans, and conclude that interstitial cells of Cajal cells lead to an abrupt transition in the motility pattern of the developing gut.

MATERIALS AND METHODS

Chicken gut samples. Fertilized chicken eggs were purchased from EARL Morizeau (Chartres, France; breeder Hubbard, JA57 hen, I66 rooster, yielding type 657 chicks). The eggs were incubated at 37.5°C in a humidified chamber for 7–16 days. The gastrointestinal tracts were dissected from hindgut to stomach; the mesentery and Remak's nerve were removed.

Whole mount in situ hybridization. Whole mount in situ hybridization analyses were carried out as described using newly isolated antisense ANO1 riboprobes (4, 12), SOX10 (4), and SM22 (11). Chick ANO1 cDNA, also known as TMEM16A or DOG1, was isolated from E6 stomach RNA extract using a specific primer pair of predicted chick ANO1 (Gene Bank ID: XM_004941529.3; forward 5'-AAG AGA AAG CAG ATG CGG-3', reverse 5'-GCA ACA TAG AAG ATG GGT GTG-3'). The resulting 517-base pair (bp) fragment

was cloned into the pGEM-T Easy plasmid (Invitrogen) and sequenced to verify identity. Dissected GI tissues were fixed in 4% paraformaldehyde for 1 h at room temperature, washed in PBS, and gradually dehydrated in methanol to store the samples at -20°C for at least one night. For whole mount in situ hybridization experiments, tissues were gradually rehydrated in PBS, washed in PBT (PBS, 0.1% Tween), and incubated for 1 h in 6% hydrogen peroxide (Sigma). Samples were next permeabilized by treatment with proteinase K (10 µg/mL) for 10 min, washed with glycine in PBT, and fixed in 4% paraformaldehyde-0.2% glutaraldehyde in PBT for 20 min. Tissues were then hybridized with antisense ANO1 digoxigenin-labeled (Roche) riboprobes overnight at 70°C. After posthybridization washes at 70°C, tissues were incubated in 10% sheep serum for 2.5 h at room temperature and finally mixed with preabsorbed antidigoxigenin coupled with alkaline phosphatase antibody (Roche) overnight at 4°C. The complexes were detected with BM Purple, a chromogenic substrate for alkaline phosphatase (Roche). Whole gut images (Fig. 1A) were acquired with a Canon D500 digital camera fixed to a tripod; magnified images (Fig. 1C and Supplemental Fig. S2; Supplemental Material for this article can be found online at <https://doi.org/10.6084/m9.figshare.12090681.v1>) were obtained by pressing excised ~1-cm-long gut segments between two microscope glass slides spaced out by 200 µm. The compressed guts were imaged with an inverted Leica microscope in DIC (differential interferential contrast) mode.

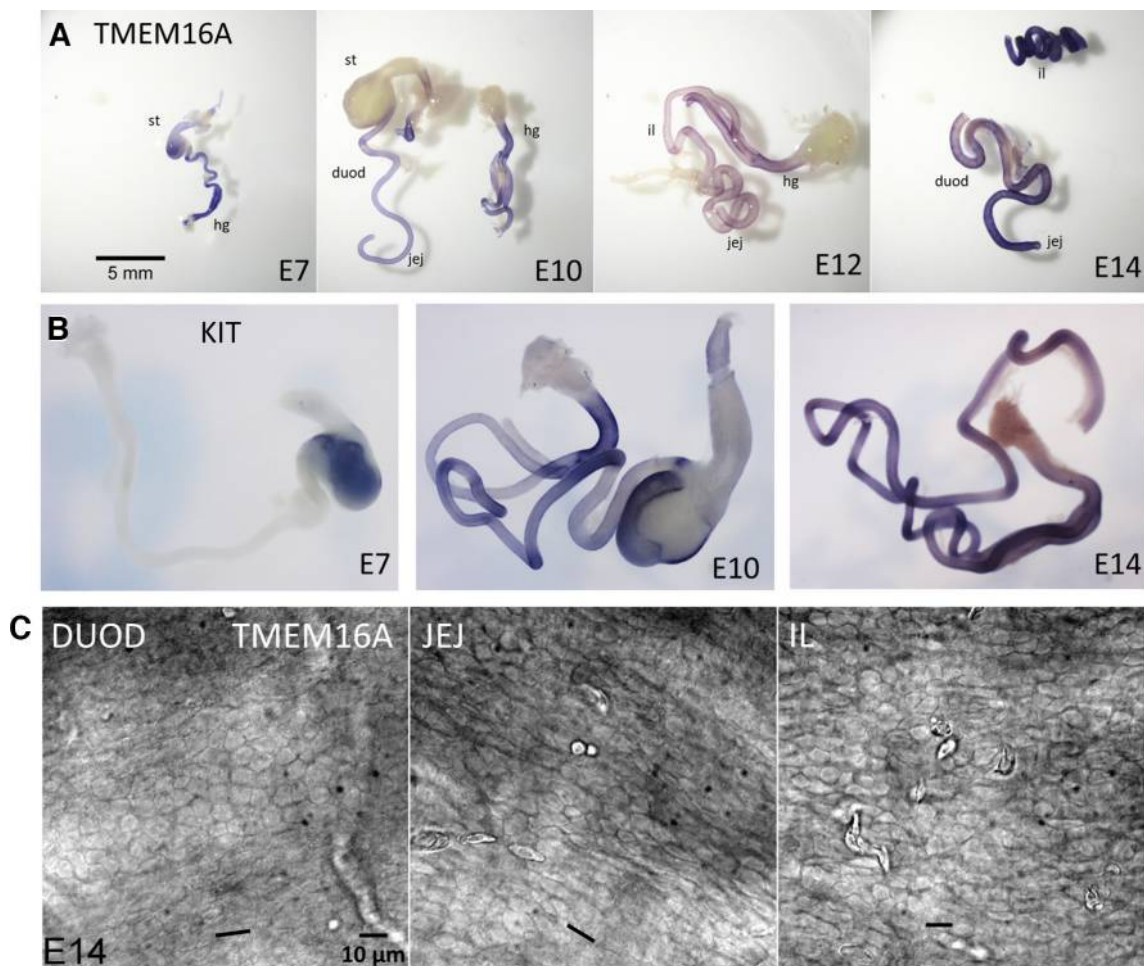


Fig. 1. Anoctamin-1 (ANO1) (TMEM16A) and KIT in situ hybridization. *A*: whole mount images for ANO1. *B*: whole mount images for KIT. *C*: magnified regions of TMEM16A staining imaged by differential-interferential contrast in the duodenum (duod), jejunum (jej), and ileum (il) on embryonic day (E)14. Scale bar is the same for all images; black line indicates the rostro-caudal axis. hg, Hindgut; st, stomach.

Quantitative real-time RT-PCR. Total RNA was extracted from cultured intestines with or without Imatinib with the HighPure RNA Isolation Kit (Roche). Reverse transcription (RT) was performed using the Verso cDNA Synthesis Kit (Thermo Scientific), and quantitative real-time PCR was performed using the LightCycler technology (Roche Diagnostics). PCR primers (Supplemental Fig. S3) were designed using the LightCycler Probe Design software-2.0. Four individual intestines were individually analyzed for each condition. Levels of *KIT*, α *SMA*, *SM22*, and *SOX10* transcripts were determined with the LightCycler analysis software (version 3.5) relative to standard curves. Data were presented as the expression levels of *KIT*, α *SMA*, *SM22*, and *SOX10* relative to the expression of the reference genes GAPDH and RPLPO. The relative mRNA expression was calculated using the $2^{-\Delta\Delta CT}$ method (12, 25).

Calcium imaging. One-centimeter-long segments from the proximal half of the midgut (duodenum and jejunum) were collected. For

calcium indicator loading, 50 μ g of Fluo4-AM (F14201; ThermoFisher) was dissolved in 10 μ L DMSO; this solution was added to 2 mL of DMEM GlutaMAX (4.5 g/L D-glucose, sodium pyruvate, Ca^{2+} 1.8 mM, Mg^{2+} 0.8 mM; ThermoFisher) containing 1% penicillin-streptomycin (PS), 25 mM HEPES, and 0.1% Kolliphor EL (Sigma). Each segment was placed in a separate well containing 200 μ L of this loading solution in a 12-well plate; the atmosphere above the wells was maintained at 95% O_2 -5% CO_2 by constant perfusion of the plate with carbogen, in a 37°C incubator. Samples were incubated for 4 h; this unusually long incubation time, as well as the high Kolliphor concentration (0.1%), was key to reliably obtaining a signal in ICCs in this whole mount preparation protocol. When comparing the calcium activity at different ages (Fig. 2C), gut segments of different aged embryos (E12–E16) were incubated in the same loading solution and plate, and their activity was compared after a 4-h incubation.

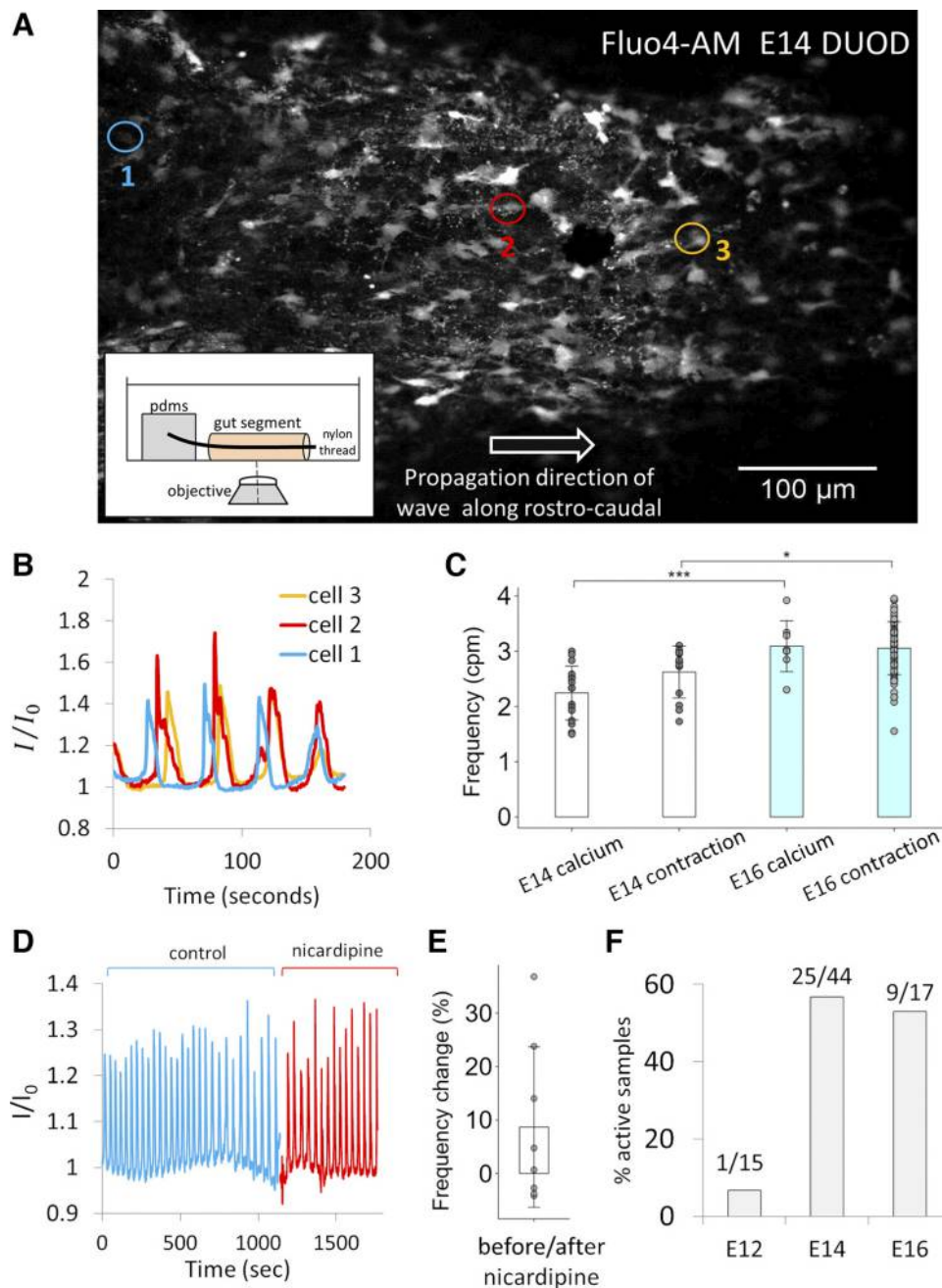


Fig. 2. Calcium activity in interstitial cells of Cajal (ICCs). **A**: still image from Supplemental Video S1, embryonic day (E)14 duodenum. The ICCs appear as brighter cells with a stellate morphology. **Inset**: setup to immobilize the gut for calcium imaging. The nylon thread inserted in the lumen gently presses the gut against the dish bottom. **B**: fluorescence (calcium) dynamics in 3 cells circled in **A**, showing both the rhythmic and propagative nature of the transients. **C**: comparison of the frequency of calcium spikes recorded by calcium imaging and of the contraction frequency obtained from video recording of guts in a physiological bath. Each dot is a different sample. *Statistically significant difference, $P < 0.05$, 1-way ANOVA test. *** $P < 0.01$. **D**: representative effect of nicardipine on calcium oscillations. **E**: frequency change induced by nicardipine for $n = 7$ samples of E14 duodenum and proximal jejunum from $n = 4$ different embryos. The frequency change is not significantly different from 0. **F**: %active samples for E12, E14, and E16 embryos. No. of embryos at each stage is $n = 5$ on E12, $n = 13$ on E14, and $n = 7$ on E16. An active sample is defined as having at least 1 region with 1 cell showing sustained fluorescence oscillations. Images in **C** and **E** were produced with the GraphRobot (36).

Immobilization of the samples for imaging is illustrated in Fig. 2A, *inset*. A thin plastic rod (nylon fishing thread, 150- μ m diameter for E12, 200 μ m for E14 and E16) was inserted in the lumen of each segment, and one end of the rod was pinned to an \sim 1-cm³ slab of PDMS secured to the bottom of a 35-mm Petri dish. The rod delicately pressed the preparations against the petri dish. Friction of the gut with the dish prevented excessive motion of the cells due to gut contractions. Samples were imaged with an inverted spinning-disk confocal microscope (Olympus or Zeiss) at magnification \times 20, laser excitation 488 nm, emission filter 512 nm, and 2-Hz imaging frequency, at 37°C. Images were collected from one confocal plane (no z-stack). The samples were immersed in 3 mL of DMEM that had been saturated with carbogen just before sample imaging. For experiments with L-type calcium channel blockers, time lapse was set for \sim 10 min; nicardipine (10 μ M) was added after \sim 5 min of recording. Resulting movies and calcium fluctuations were analyzed with ImageJ.

Recording of contractile activity. Physiological bath video recordings of gut activity were performed, following previously established techniques (6). Briefly, gut segments were pinned vertically to the wall of a Sylgard-lined chamber filled with 40 mL of DMEM at 37°C constantly bubbled with carbogen. Guts were recorded with a video camera (1-Hz time lapse) after a 30-min equilibration period; up to six segments were recorded simultaneously. The contractile activity, speed and frequency, was analyzed using spatiotemporal maps and the ImageJ “reslice” function on rectangular regions of interest (ROIs) encompassing the gut segments (6, 7). The speed was sometimes directly measured from the movie when a good quality map could not be obtained. Acute effects of imatinib mesylate (Sigma) were tested by adding increasing concentrations from a 14.4 mg/mL concentrate solution in DMSO.

Organ culture. Immediately after dissection, E12 proximal midguts (duodenum ad jejunum) were cut in \sim 1-cm-long segments, and the segments were alternatively placed in the control medium (DMEM + 0.04% DMSO) or in the imatinib medium (DMEM + 10 μ M imatinib). This procedure guaranteed that control and imatinib-treated sample pairs originated from the same gut region and, therefore, initially had similar contractile properties. Each segment was placed in 1 mL of medium in a 35-mm petri dish; all samples were incubated at 37°C in a 95% O₂ + 5% CO₂ atmosphere by constant carbogen perfusion. We previously (17) found this atmosphere to be suitable for chicken fetal gut development and growth. Medium and drug were replaced after 1.5 days of culture. After 3 days of culture, the contractile activities of the control and imatinib-treated segments were monitored in the physiological bath setup described above.

RESULTS

Interstitial cells of Cajal are present throughout the chicken GI tract as from E7. We detected the presence of interstitial cells of Cajal by in situ hybridization for the surface receptor ANO1 (also called TMEM16A) and KIT. The ANO1 chloride channel has been shown in the mouse (13) to be a specific maker of ICCs. ANO1-positive cells were present in the entire lower GI tract (duodenum, jejunum, ileum, hindgut, and ceca) as from E7 and at all later stages (Fig. 1A). The number of guts stained were as follows: E7, $n = 5$; E8, $n = 3$; E9, $n = 3$; E10, $n = 3$; E12, $n = 4$; E14, $n = 2$. The stomach was stained only in the muscular region; the mesentery, the cloaca, and any remaining umbilical stalk tissue were not stained. KIT staining could only be detected as from E10 (Fig. 1B). ANO1 and KIT staining patterns were identical as from E10.

Higher-magnification differential-interferential contrast (DIC) imaging of the ANO1 in situ hybridized guts showed a net of dark, interconnected cells that were located just above the circular muscle layer and elongated along the rostro-caudal axis of the

gut (Fig. 1C). On E14, the longitudinal layer was differentiated, and we could confirm that the ANO1-positive cells were located between the longitudinal and circular muscle layers, i.e., at the level of the myenteric plexus (MP). Therefore, these ANO1-positive cells are ICC-MP. The ICCs presented similar morphologies at E10 (Supplemental Fig. S2).

A specific calcium-sensitive dye whole mount loading protocol reveals the electrical activity of ICCs. We next devised a protocol to monitor the calcium activity of ICCs with the calcium-sensitive probe Fluo4-AM. Short-time (10 min) application of this dye to transverse sections of early (E9) embryonic gut had allowed us to visualize calcium waves propagating across the contractile smooth muscle layer (5). Here, we loaded \sim 1-cm-long whole mount segments of demensenterized E12–E14 guts at the same concentration, but for significantly longer times (4 h) and in the presence of higher (0.1%) quantities of the cell permeant Kolliphor EL (for details, see MATERIALS AND METHODS). The samples were immobilized as shown in Fig. 2A, *inset* (see MATERIALS AND METHODS for details). A representative video of the calcium activity observed following this preparation is shown in Supplemental Video S1.

Active (i.e., presenting a time-dependent fluorescence) cells had a stellate morphology and were slightly elongated along the rostro-caudal axis of the gut (Fig. 2A). They formed a discontinuous net, probably because of nonuniform penetration of the calcium dye. We found that the calcium activity consisted of regular spikes of fluorescence that propagated along the rostro-caudal axis (Fig. 2B). Although the explants presented contractions (see Supplemental Video S1), the active cells were not contractile. The frequency of calcium oscillations at ages E14 (2.2 ± 0.5 cycles/min; $n = 16$ samples from $n = 9$ embryos, uncertainty is \pm SD) and E16 (3.1 ± 0.5 cycles/min; $n = 8$ samples from $n = 5$ embryos) corresponded to the frequency of circular smooth muscle contractions as recorded in a physiological bath at these two stages (Fig. 2C). In particular, the calcium spike frequency was significantly higher on E16 than on E14, just like the circular contraction frequency (Fig. 2C). We further found that the oscillations were insensitive to nicardipine (Fig. 2, D and E), a Ca²⁺ L-type channel blocker. This is unlike smooth muscle calcium transients, which critically depend on L-type channels (17). Independence on L-type calcium channel is a characteristic of oscillations in ICCs (20).

Fluo4-AM penetrated in the ganglia and interganglionic fibers of the myenteric plexus (MP) so that the morphology of this part of the enteric nervous system could be clearly visualized following calcium dye loading (Supplemental Video S2). However, none of the ganglia or interganglionic fibers presented any activity; i.e., the fluorescence labeling was constant in time. Importantly, the active cells were in the same plane as the myenteric plexus but never colocalized with ENS structures. On the basis of the morphological and physiological characteristics of the transients and of the cells that produced them (summarized in Table 1), we can conclude that the active cells are neither smooth muscle, nor enteric neurons, nor glia, and can only be stellate-shaped pacemaker ICC-MP present at the level of the myenteric plexus.

Propagating calcium activity in ICCs can first be detected on E14. We examined the calcium activity of ICCs at ages E12, E14, and E16. We defined a sample as active if it presented at least one cell with sustained oscillations after examining three different regions of the sample. The same protocol for calcium

Table 1. *Properties of cells observed compared with other cells in the intestines*

	Morphology	Orientation	Frequency of Transients, cycles/min	Nicardipine Sensitivity	Radial Localization	Colocalization With ENS?
Circular smooth muscle	Fusiform	Circular	1.5–3	Yes	Below MP	No
Longitudinal smooth muscle	Fusiform	<i>Longitudinal</i>	0.2–0.4	Yes	Above MP	No
ENS	Ganglion network	Honeycomb			<i>At MP</i>	Yes
ICC-MP	<i>Stellate</i>	<i>Longitudinal</i>	1.5–3	No	<i>At MP</i>	No
Cells observed	Stellate	Longitudinal	1.5–3	No	At MP	No

ENS, enteric nervous system; ICC, interstitial cells of Cajal; MP, myenteric plexus. Italics indicate correspondence with properties of the cells we observed in Fig. 1.

indicator loading was applied to all samples so that their activity could be compared; E12 and E14 guts were loaded on the same days and in the same 12-well plate. Activity could be detected in one of 15 samples on E12, in 25 of 44 samples on E14, and in nine of 17 samples on E16 (Fig. 2F).

Activation of ICCs is concomitant with a change of contractile wave speed, frequency, and regularity. We next examined the contractile wave pattern on E12 and E14, at the time where calcium activity in ICCs was first observed. Spatiotemporal diagrams on E12 and E14 show conspicuous differences (Fig. 3A). Contractile waves on E12 are multidirectional, irregular, and relatively slow. In contrast, on E14, they become regular, keep the same direction for prolonged periods of time, and travel at a relatively higher speed. By compounding data from experiments at the embryonic (7) and fetal (6) stages, we found that the frequency of contractile waves increased linearly between E8 and E16, at a rate of $0.22 \text{ cycles} \cdot \text{min}^{-1} \cdot \text{day}^{-1}$ (Fig. 3B). The speed

of contractile waves exhibited a pronounced discontinuity between E12 and E14 (Fig. 3C), increasing from $25 \mu\text{m/s}$ to $125 \mu\text{m/s}$, a fivefold difference.

Specific ICC inhibition by imatinib mesylate abolishes the transition to ICC-driven motility on E12–E14. We finally asked whether the transition to regular contractile waves happening between E12 and E14 could be inhibited by specifically targeting ICCs. Imatinib mesylate is a known inhibitor of the c-KIT surface receptor and has been successfully used to inhibit ICC development in the mouse by Beckett et al. (3). We first examined the effects of imatinib on ICCs, smooth muscle cells, and the ENS by performing in situ hybridization and RTqPCR on E12 intestines cultured for 3 days in the presence or in the absence of imatinib (Fig. 4). We placed 1- to 2-cm-long segments of E12 alternately in control medium (with vehicle only) or in $10 \mu\text{M}$ imatinib medium; this procedure guaranteed that control and drug-treated samples were from the same rostral-caudal

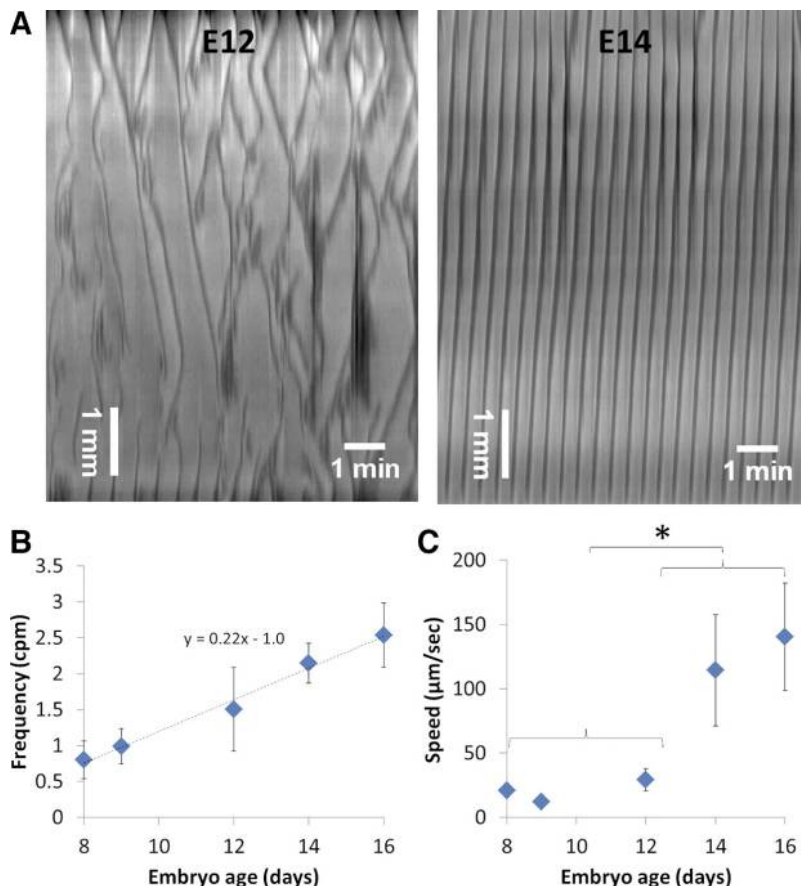


Fig. 3. A transition to regular, rhythmic, and higher-speed contractile waves occurs between embryonic day (E)12 and E14. **A**: representative spatiotemporal maps on E12 and E14 duodenum. **B**: evolution of contractile wave frequency from E8 to E16 in the jejunum. Embryo numbers: E8, $n = 8$; E9, $n = 7$; E12, $n = 6$; E14, $n = 14$; E16, $n = 42$. Formula and dashed line are a linear fit of the data. Error bars are SD. **C**: evolution of contractile wave speed. Embryo number is the same as in **A**, except that $n = 11$ on E16. Error bars are SD. *Statistically significant difference, $P < 0.05$, Mann-Whitney 2-tailed test. All statistical comparisons are performed between 2 sample populations.

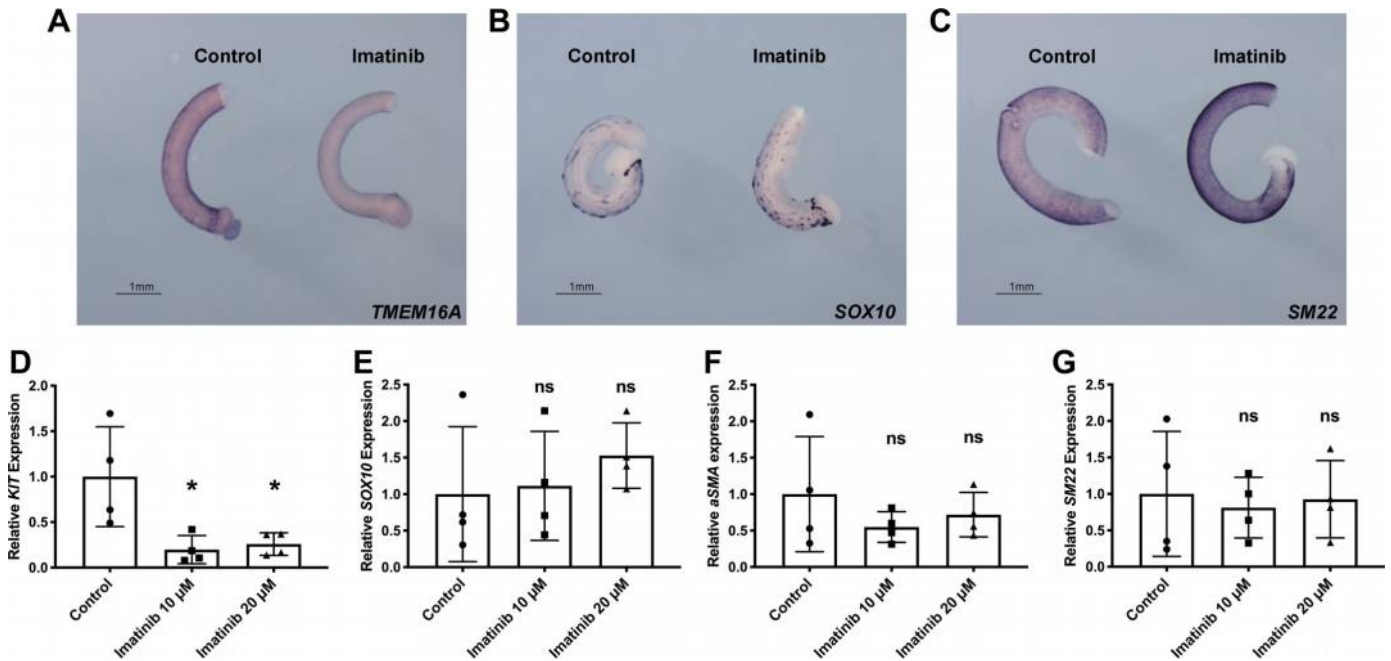


Fig. 4. Whole mount in situ hybridization of embryonic day (E)12 intestine treated or not with imatinib (10 μ M) for 3 days. Control (A–C, left) and imatinib-treated (A–C, right) intestines were processed for TMEM16A (A), SOX10 (B), and SM22 (C) riboprobes. TMEM16A staining is lower in imatinib-treated intestine compared with control segment. Enteric nervous system (ENS) network (SOX10 staining) and smooth muscle (SM22 staining) are unaffected upon imatinib treatment. D–G: quantification of transcript levels by RT-quantitative PCRs in control and imatinib-treated intestines (10 μ M and 20 μ M). Imatinib treatments induce a decrease in the level of KIT (D). No significant changes were observed in the level of SOX10 (ENS marker; E) or aSMA/SM22 (smooth muscle marker; F and G). Data were normalized to GAPDH and 60S acidic ribosomal protein P0 (RPLP0) expression. Normalized expression levels were converted to fold changes. NS, not significant. Values are presented as the mean SD of $n = 4$, control; $n = 4$, 10 μ M and 20 μ M imatinib-treated intestines. * $P < 0.05$ by 2-tailed Mann-Whitney tests; comparisons are performed with the control condition. L. A. Wang produced the images in B with the GraphRobot (36) that he developed.

region along the GI tract (see MATERIALS AND METHODS). Imatinib treatment induced a decrease in the level of TMEM16A (Fig. 4A) and KIT transcripts (Fig. 4D), suggesting a decrease in the number of ICCs. No significant changes were observed on the transcript levels of SOX10 (Fig. 4, B and E) and SMC-specific genes, such as α -SMA (Fig. 4F) and SM22 (Fig. 4, C and G), indicating that the ENS network and the smooth muscle cells were not affected by imatinib.

We then examined the effects of imatinib on motility. We first tested the acute effects of this drug on contractile activity at E14, when ICCs were already active. We found that imatinib at concentrations of 1 μ M and 10 μ M did not have any acute effects on the contractile wave pattern ($n = 5$ samples, E14 duodenum; Fig. 5A) for ≤ 30 min. This indicates that imatinib at these concentrations does not have an immediate action on ion channels that mediate contractility (e.g., calcium channels). Imatinib did, however, have a marked effect when applied for 3 days on E12 guts in culture, in the critical period when ICCs become active. In control samples ($n = 18$ samples), the frequency (Fig. 5E) and contractile wave speed (Fig. 5F) significantly increased after 3 days of culture, reflecting the physiological changes happening in ovo (Fig. 3, B and C). In particular, the contractile wave pattern of control samples after culture exhibited a high degree of regularity and directionality (Fig. 5B, top), like E14 intestines (Fig. 3A). This echoes findings by other investigators that the ICC network develops normally in cultured, isolated mouse intestines (38).

The contractile pattern of imatinib-treated samples was characterized by a conspicuous lack of rhythmicity (Fig. 5B,

bottom). We characterized this by performing time Fourier transforms of the spatiotemporal diagrams (Fig. 5C). Whereas control samples presented a distinct peak (black arrowhead) with harmonics, the peak was either weak and broad in five of 18 or nonexistent in 13 of 18 imatinib-treated samples. The intensity of the Fourier peak was significantly reduced in imatinib-treated samples (Fig. 5D). Motility in imatinib samples were characterized by long periods of quiescence, interspersed by single or trains of contractions. The average frequency between trains of contractions was 0.9 ± 0.7 cycles/min ($n = 18$ samples; Fig. 5E) and was significantly lower than in controls (2.9 ± 1.3 cycles/min). The contraction velocity was higher in imatinib-treated samples (418 ± 316 μ m/s; Fig. 5F) than in their control counterpart (266 ± 270 μ m/s), although this was not statistically significant. Supplemental Video S3 illustrates the contractile activity of a pair of control and imatinib-treated guts after 3 days in culture. We also tested whether imatinib could have side-effects on E7 guts cultured for 3 days, i.e., at a time interval where ICCs are presumably not yet active. We found that the spatiotemporal maps, frequency, and speed of contractile waves in control and imatinib-treated samples did not differ (Supplemental Fig. S1), indicating that imatinib 10 μ M did not affect purely myogenic (smooth muscle-driven) contractility.

DISCUSSION

We showed by in situ hybridization for the cell surface receptor ANO1 that ICCs are present at least as from E7 in the whole lower gastrointestinal tract of the chicken and presented the first

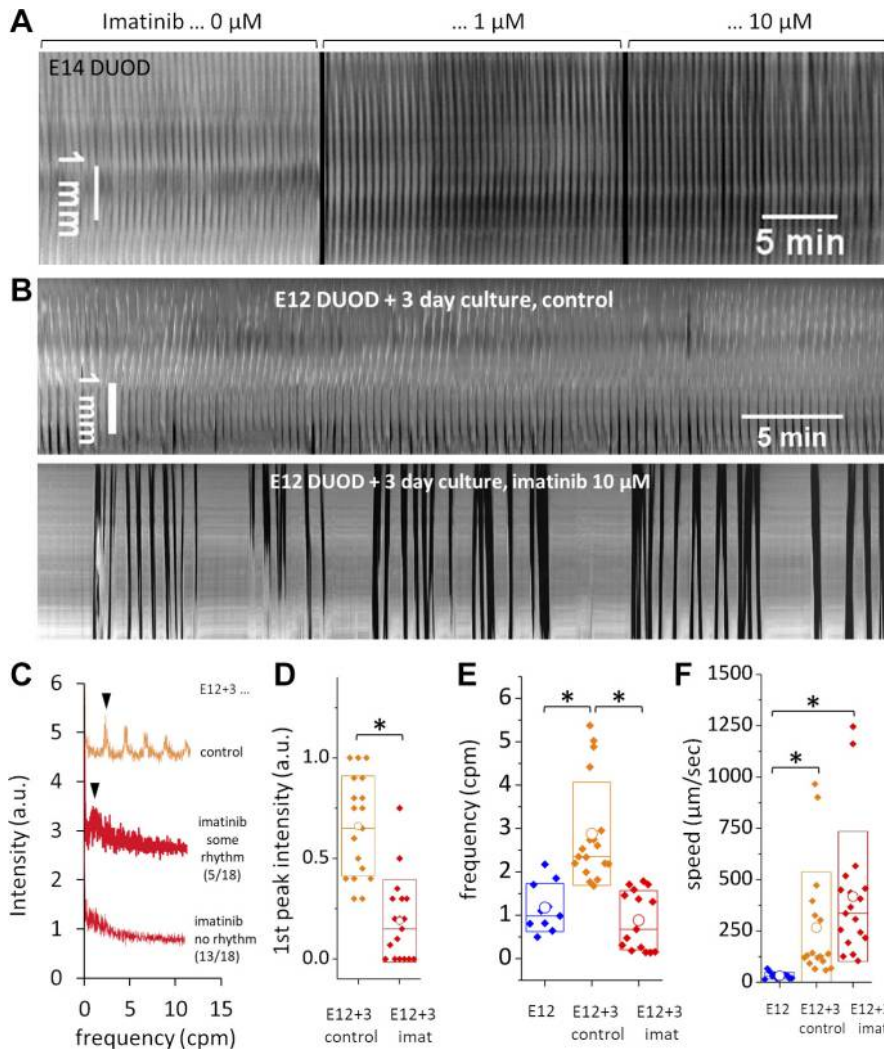


Fig. 5. Effect of imatinib mesylate on the motility during the Cajal transition. *A*: representative spatiotemporal maps of acute effects probed on embryonic day (E)14 duodenum (DUOD; $n = 5$ embryos probed). *B*: spatiotemporal maps of control ($n = 18$ of 18) and imatinib-treated segments featuring very irregular contractions ($n = 13$ of 18). *C*: representative Fourier transforms of a horizontal line along the spatiotemporal diagram of control and imatinib-treated samples. *D*: compared intensity of the first peak of the Fourier transform ($n = 18$ control, $n = 18$ imatinib). *E* and *F*: evolution of the frequency and speed of contractile waves on E12 ($n = 10$) and after 3-day culture of the midgut segments in DMEM with vehicle alone (control, DMSO, $n = 18$) or in imatinib 10 μM ($n = 18$). *Statistically significant difference, $P < 0.05$, 2-tailed Mann-Whitney test. AU, arbitrary units. n , number of samples.

images of this cell network in the avian embryonic gut (Fig. 1). We next devised a protocol for whole mount calcium indicator loading of gut explants that allowed us to record what we identified as ICC oscillatory and propagative calcium activity (Fig. 2). We found that calcium activity in ICCs starts at E14. Comparison of the contractile wave activity on E12 and E14 shows that the start of ICC activity coincides with the onset of rhythmic and coordinated contractions that propagated as a coherent wavefront along the intestine, with a stabilization of contractile wave rhythm, propagation direction, and also with an increased propagation speed (Fig. 3). Subjecting E12 guts to the c-KIT inhibitor imatinib mesylate in culture depleted ICCs (Fig. 4) and abolished the physiological transition to regular, rhythmic contractile waves (Fig. 5).

Lecoin et al. (19) were the first to perform c-KIT radioactive probe in situ hybridization in the chicken embryonic gut. They found a weak signal on E7 and provided cross-section images at E9, indicating the presence of c-KIT-positive cells at this stage. Using alkaline phosphatase detection to reveal KIT and ANO1 in situ hybridization, we found that KIT was present in the entire GI tract on E10 but not E7 and that ANO1-positive cells were present at least as from E7, i.e., at the same time or soon after

smooth muscle differentiation on E5 and E6 (4, 7, 25). This difference between KIT and ANO-1 may be due to the fact that transcriptional levels of ANO-1 in ICCs are known to be higher than for KIT (23). Our results are consistent with studies in the mouse (3, 30), where ICCs were found as from E14.5, i.e., only a day after smooth muscle differentiation in the midgut at E13.5. We found that ICCs organize as a continuous net, located at the level of the myenteric plexus. The morphology of the ICC network in chicken resembles that revealed by antibody labeling in the mouse embryo (3, 30, 38); this is unlike the enteric nervous system, which has a very different morphology in these two species.

Ca^{2+} imaging has been used to visualize the activity of ICCs in numerous investigations (1, 2, 26, 39), but the results presented here are to the best of our knowledge the first in situ calcium recordings of ICCs in a developing organism and in particular of their very first glimpses of activity in this organism's life. We have found that sustained calcium electrical oscillations start in these cells at stage E14. Electrophysiological recordings indicate that the first slow waves in the mouse intestine arise at stages E18 and E19 (3, 30) and are fully developed by 2 days after birth (22). These developmental times are

consistent with the 4- to 7-day advance of developmental events in the chicken embryo compared with the mouse (see the table in Ref. 6 for examples). We summarize important milestones in the development of gut motility in the chicken in Fig. 6, *top*. Given the week/day equivalence of human and chicken intestinal development (6), we predict that a transition to ICC-driven motility should take place between 12 and 14 wk of development in the human embryo.

We found that the appearance of calcium activity in ICCs on E14 led to drastic changes in the circular smooth muscle contractile wave pattern; waves became more rhythmic (more regular), kept the same direction for prolonged periods of time, and had an increased propagation speed (from 25 $\mu\text{m/s}$ to 125 $\mu\text{m/s}$ from E12 to E14). Several methods have been developed to deplete or inactivate the ICC network: irradiation after methylene blue staining (21), antibodies directed towards c-KIT (3, 35, 38), imatinib mesylate (3), and, last but obviously not least, the W/W^V mutant, which lacks the c-KIT receptor (24, 37). All of these alterations have been shown to suppress slow waves in the murine gut. The W/W^V mutant is viable, and the effects of ICC depletion on GI motility in the adult mouse have been examined by radiography of barium sulfate-gavaged mice and subsequent electrophysiology and manometry (9). These investigators found that whereas contractions in control mice were rhythmic and pushed the contrast fluid aborally, movements in W/W^V mice were erratic, with irregular smooth muscle action potentials traveling both orally and aborally, leading to weakened overall bolus propulsion. This picture resonates with the erratic contractile wave pattern we obtained after treatment of E12 gut with the c-KIT inhibitor for 3 days (Fig. 5B). Parsons and Huizinga (28) recently reported spatiotemporal D-maps of

W/W^V and of the W^{sh}/W^{sh} mouse; they found very high-velocity (“lines of simultaneity”), irregular, and multidirectional contractions. The overall frequency of the contractions was approximately three times lower in these mutants ($\sim 10\text{--}15$ cycles/min) than in control mice (~ 45 cycles/min). Our results are in line with these findings, as we also found that the E12 guts treated with imatinib for 3 days (and which hence, are a model of a gut with dysfunctional ICCs) present very high-velocity, irregular contractions. Physiologically, ICC activation on E14 coincides with a sharp increase in the velocity of contractile waves compared with E12 (Fig. 3C). We speculated that this increase may be due to the transition from a trigger-wave regime (27) at early embryonic stages (E7–E12) to an ICC-driven phase wave (27) regime at fetal stages (E14+). Because waves in chains of coupled oscillators depend on electrical phase coupling between adjacent cells, we intuited that they may propagate at higher speeds than trigger waves. Therefore, we expected ICC inhibition by imatinib to result in a lower propagation speed compared with controls, but it is in fact the opposite that we observed. Therefore, the increased speed of contraction between E12 and E14 may not be a direct consequence of ICC activation but rather involve other phenomena like increased gap junction conductance. As a matter of fact, very early E5 and E6 embryonic gut (7), W/W^V mice (28), or vascular smooth muscle (29) also feature very high-velocity contractions, but none of them contain active ICCs.

ICCs and smooth muscle are closely related, as they both originate from the mesoderm (19), and simply blocking c-KIT signaling has been shown to revert ICCs to a smooth muscle phenotype (34). This plasticity reinforces the view that the early smooth muscle mesenchyme (E6–E12) should be viewed as one

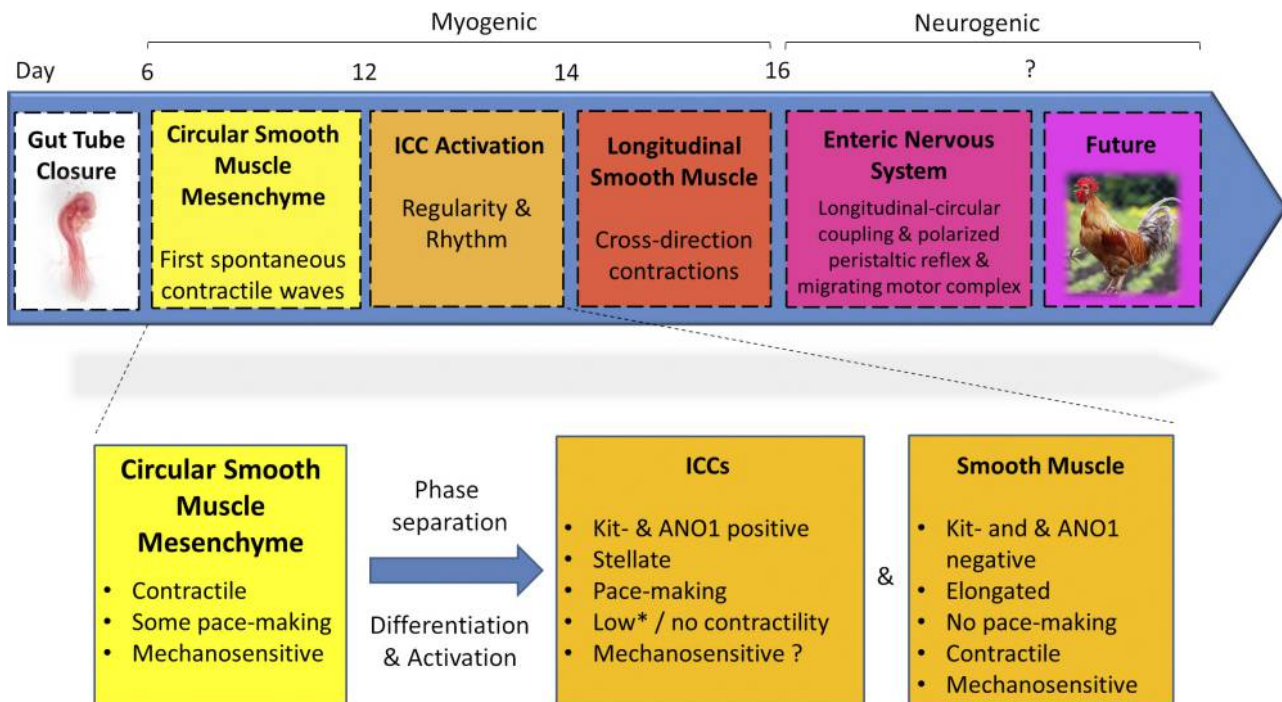


Fig. 6. *Top*: important milestones in the development of gut motility in the chicken embryo. Given the observed week/day equivalence (6) of many of these events in human and chicken intestinal development, a similar timeline is expected to hold for the human embryonic gut in weeks of development. *Bottom*: focus on the underlying cellular differentiation events that underpin the ICC motility transition. *Some contractility in interstitial cells of Cajal (ICCs) has been observed by Huizinga et al. (14) but remains to be confirmed. ANO1, anoctamin-1.

unit that has both contractile and contraction-initiating (pacemaking) properties (Fig. 6, *bottom*). It separates in a KIT- and ANO1-positive (ICCs) and a KIT- and ANO1-negative population (smooth muscle). The first population (ICCs) loses the ability to contract and specializes in generating the regular electrical impulses that initiate contractions. The second (smooth muscle) in turn loses the ability to generate its own regular electrical impulses and retains contractility. Although ICCs can be observed as from E7, they only become active in the interval E12–E14. This phase separation and subsequent activation (Fig. 6, *bottom*) drives a major change in the rhythmicity and directionality of contractions. In contrast, spatio-temporal maps from E6 to E12 were qualitatively quite similar. Therefore, we suggest the term “ICC transition” to refer to this abrupt motility regime change happening in the developing fetal gut. Important questions are: how common is this separation in the contractile versus pacemaking population in other smooth muscle-lined organs (15) or in cancer tumors (8)? What factors trigger this separation? Later in gut development the enteric nervous system becomes active (on E16 in the chicken and E18.5 in the mouse), triggering the emergence of the migrating motor complex (6, 30) and of the asymmetric ascending-contraction descending-inhibition barometric reflex (6). Because different cell types become active at distinct times during ontogenesis, the developing embryo represents a unique laboratory to understand the sequence of events and the mechanisms leading to mature physiological reflexes.

ACKNOWLEDGMENTS

We thank Xavier Baudin and Nicolas Moisan from the ImagoSeine facility (Jacques Monod Institute, Paris, France) and the France bioimaging infrastructure supported by the French National Research Agency (ANR-10-INSB-04, “Investments of the Future”) for precious help with high-resolution confocal microscopy for calcium imaging. We thank Lei A. Wang for the GraphRobot that was used to produce the images in Figures 2, C and E, and 4B.

GRANTS

This research was funded by the Agence Nationale de la Recherche ANR GASTROMOVE-ANR-19-CE30-0016-01 and by the Université de Paris IDEX Emergence en Recherche CHEVA19RDX-MEUP1.

DISCLOSURES

No conflicts of interest, financial or otherwise, are declared by the authors.

AUTHOR CONTRIBUTIONS

N.R.C. conceived and designed research; N.R.C., Y.A., A.G., C.T., P.d. and S.F. performed experiments; N.R.C., Y.A. and A.G. analyzed data; N.R.C. and Y.A. interpreted results of experiments; N.R.C. and Y.A. prepared figures; N.R.C. drafted manuscript; N.R.C., P.d. and S.F. edited and revised manuscript; N.R.C., Y.A., A.G., C.T., P.d. and S.F. approved final version of manuscript.

REFERENCES

- Baker SA, Drumm BT, Saur D, Hennig GW, Ward SM, Sanders KM. Spontaneous Ca(2+) transients in interstitial cells of Cajal located within the deep muscular plexus of the murine small intestine. *J Physiol* 594: 3317–3338, 2016. doi:10.1113/JP271699.
- Bayguinov PO, Hennig GW, Smith TK. Ca2+ imaging of activity in ICC-MY during local mucosal reflexes and the colonic migrating motor complex in the murine large intestine. *J Physiol* 588: 4453–4474, 2010. doi:10.1113/jphysiol.2010.196824.
- Beckett EAH, Ro S, Bayguinov Y, Sanders KM, Ward SM. Kit signaling is essential for development and maintenance of interstitial cells of Cajal and electrical rhythmicity in the embryonic gastrointestinal tract. *Dev Dyn* 236: 60–72, 2007. doi:10.1002/dvdy.20929.
- Bourret A, Chauvet N, de Santa Barbara P, Faure S. Colonic mesenchyme differentiates into smooth muscle before its colonization by vagal enteric neural crest-derived cells in the chick embryo. *Cell Tissue Res* 368: 503–511, 2017. doi:10.1007/s00441-017-2577-0.
- Chevalier NR. The first digestive movements in the embryo are mediated by mechanosensitive smooth muscle calcium waves. *Philos Trans R Soc Lond B Biol Sci* 373: 20170322, 2018. doi:10.1098/rstb.2017.0322.
- Chevalier NR, Dacher N, Jacques C, Langlois L, Guedj C, Faklaris O. Embryogenesis of the peristaltic reflex. *J Physiol* 597: 2785–2801, 2019. doi:10.1113/JP277746.
- Chevalier NR, Fleury V, Dufour S, Proux-Gillardeaux V, Asnacios A. Emergence and development of gut motility in the chicken embryo. *PLoS One* 12: e0172511, 2017. doi:10.1371/journal.pone.0172511.
- de Silva CM, Reid R. Gastrointestinal stromal tumors (GIST): C-kit mutations, CD117 expression, differential diagnosis and targeted cancer therapy with Imatinib. *Pathol Oncol Res* 9: 13–19, 2003. doi:10.1007/BF03033708.
- Der-Silaphet T, Malysz J, Hagel S, Arsenaault AL, Huizinga JD. Interstitial cells of cajal direct normal propulsive contractile activity in the mouse small intestine. *Gastroenterology* 114: 724–736, 1998. doi:10.1016/S0016-5085(98)70586-4.
- Farrugia G. Interstitial cells of Cajal in health and disease. *Neurogastroenterol Motil* 20, Suppl 1: 54–63, 2008. doi:10.1111/j.1365-2982.2008.01109.x.
- Faure S, Georges M, McKey J, Sagnol S, de Santa Barbara P. Expression pattern of the homeotic gene Bapx1 during early chick gastrointestinal tract development. *Gene Expr Patterns* 13: 287–292, 2013. doi:10.1016/j.ggp.2013.05.005.
- Faure S, McKey J, Sagnol S, de Santa Barbara P. Enteric neural crest cells regulate vertebrate stomach patterning and differentiation. *Development* 142: 331–342, 2015. doi:10.1242/dev.118422.
- Huang F, Rock JR, Harfe BD, Cheng T, Huang X, Jan YN, Jan LY. Studies on expression and function of the TMEM16A calcium-activated chloride channel. *Proc Natl Acad Sci USA* 106: 21413–21418, 2009. doi:10.1073/pnas.0911935106.
- Huizinga JD, Lammers WJEP, Mikkelsen HB, Zhu Y, Wang XY. Toward a concept of stretch coupling in smooth muscle: a thesis by Lars Thuneberg on contractile activity in neonatal interstitial cells of Cajal. *Anat Rec (Hoboken)* 293: 1543–1552, 2010. doi:10.1002/ar.21214.
- Hutchings G, Williams O, Cretoiu D, Ciontea SM. Myometrial interstitial cells and the coordination of myometrial contractility. *J Cell Mol Med* 13: 4268–4282, 2009. doi:10.1111/j.1582-4934.2009.00894.x.
- Huycke TR, Miller BM, Gill HK, Nerurkar NL, Sprinzak D, Mahadevan L, Tabin CJ. Genetic and mechanical regulation of intestinal smooth muscle development. *Cell* 179: P90–P105.E21, 2019. doi:10.1016/j.cell.2019.08.041.
- Khalipina D, Kaga Y, Dacher N, Chevalier NR. Smooth muscle contractility causes the gut to grow anisotropically. *J R Soc Interface* 16: 20190484, 2019. doi:10.1098/rsif.2019.0484.
- Klein S, Seidler B, Kettenberger A, Sibaev A, Rohn M, Feil R, Allescher HD, Vanderwinden JM, Hofmann F, Schemann M, Rad R, Storr MA, Schmid RM, Schneider G, Saur D. Interstitial cells of Cajal integrate excitatory and inhibitory neurotransmission with intestinal slow-wave activity. *Nat Commun* 4: 1630, 2013. doi:10.1038/ncomms2626.
- Lecoin L, Gabella G, Le Douarin N. Origin of the c-kit-positive interstitial cells in the avian bowel. *Development* 122: 725–733, 1996.
- Lee JCF, Thuneberg L, Berezin I, Huizinga JD. Generation of slow waves in membrane potential is an intrinsic property of interstitial cells of Cajal. *Am J Physiol Gastrointest Liver Physiol* 277: G409–G423, 1999. doi:10.1152/ajpgi.1999.277.2.G409.
- Liu LWC, Thuneberg L, Huizinga JD. Selective lesioning of interstitial cells of Cajal by methylene blue and light leads to loss of slow waves. *Am J Physiol Gastrointest Liver Physiol* 266: G485–G496, 1994. doi:10.1152/ajpgi.1994.266.3.G485.
- Liu LWC, Thuneberg L, Huizinga JD. Development of pacemaker activity and interstitial cells of Cajal in the neonatal mouse small intestine. *Dev Dyn* 213: 271–282, 1998. doi:10.1002/(SICI)1097-0177(199811)213:3<271::AID-AJA4>3.0.CO;2-R.
- Loera-Valencia R, Wang XY, Wright GWJ, Barajas-López C, Huizinga JD. Anol1 is a better marker than c-Kit for transcript analysis of

- single interstitial cells of Cajal in culture. *Cell Mol Biol Lett* 19: 601–610, 2014. doi:10.2478/s11658-014-0214-4.
24. **Maeda H, Yamagata A, Nishikawa S, Yoshinaga K, Kobayashi S, Nishi K, Nishikawa S.** Requirement of c-kit for development of intestinal pacemaker system. *Development* 116: 369–375, 1992. .
 25. **McKey J, Martire D, de Santa Barbara P, Faure S.** LIX1 regulates YAP1 activity and controls the proliferation and differentiation of stomach mesenchymal progenitors. *BMC Biol* 14: 34, 2016. doi:10.1186/s12915-016-0257-2.
 26. **Park KJ, Hennig GW, Lee HT, Spencer NJ, Ward SM, Smith TK, Sanders KM.** Spatial and temporal mapping of pacemaker activity in interstitial cells of Cajal in mouse ileum in situ. *Am J Physiol Cell Physiol* 290: C1411–C1427, 2006. doi:10.1152/ajpcell.00447.2005.
 27. **Parsons SP, Huizinga JD.** Phase waves and trigger waves: emergent properties of oscillating and excitable networks in the gut. *J Physiol* 596: 4819–4829, 2018. doi:10.1113/JP273425.
 28. **Parsons SP, Huizinga JD.** A myogenic motor pattern in mice lacking myenteric interstitial cells of Cajal explained by a second coupled oscillator network. *Am J Physiol Gastrointest Liver Physiol* 318: G225–G243, 2020. doi:10.1152/ajpgi.00311.2019.
 29. **Quijano JC, Raynaud F, Nguyen D, Piacentini N, Meister JJ.** Intercellular ultrafast Ca(2+) wave in vascular smooth muscle cells: numerical and experimental study. *Sci Rep* 6: 31271, 2016. doi:10.1038/srep31271.
 30. **Roberts RR, Ellis M, Gwynne RM, Bergner AJ, Lewis MD, Beckett EA, Bornstein JC, Young HM.** The first intestinal motility patterns in fetal mice are not mediated by neurons or interstitial cells of Cajal. *J Physiol* 588: 1153–1169, 2010. doi:10.1113/jphysiol.2009.185421.
 31. **Spencer NJ, Hibberd TJ, Travis L, Wiklendt L, Costa M, Hu H, Brookes SJ, Wattoo DA, Dinning PG, Keating DJ, Sorensen J.** Identification of a rhythmic firing pattern in the enteric nervous system that generates rhythmic electrical activity in smooth muscle. *J Neurosci* 38: 5507–5522, 2018. doi:10.1523/JNEUROSCI.3489-17.2018.
 32. **Spencer NJ, Hu H.** Enteric nervous system: sensory transduction, neural circuits and gastrointestinal motility. *Nat Rev Gastroenterol Hepatol* 17: 338–351, 2020. doi:10.1038/s41575-020-0271-2.
 33. **Spencer NJ, Sanders KM, Smith TK.** Migrating motor complexes do not require electrical slow waves in the mouse small intestine. *J Physiol* 553: 881–893, 2003. doi:10.1113/jphysiol.2003.049700.
 34. **Torihashi S, Nishi K, Tokutomi Y, Nishi T, Ward S, Sanders KM.** Blockade of kit signaling induces transdifferentiation of interstitial cells of cajal to a smooth muscle phenotype. *Gastroenterology* 117: 140–148, 1999. doi:10.1016/S0016-5085(99)70560-3.
 35. **Torihashi S, Ward SM, Nishikawa S, Nishi K, Kobayashi S, Sanders KM.** c-kit-dependent development of interstitial cells and electrical activity in the murine gastrointestinal tract. *Cell Tissue Res* 280: 97–111, 1995. .
 36. **Wang LA.** *GraphRobot* (Online). <https://www.graphrobot.com>, 2019.
 37. **Ward SM, Burns AJ, Torihashi S, Sanders KM.** Mutation of the proto-oncogene c-kit blocks development of interstitial cells and electrical rhythmicity in murine intestine. *J Physiol* 480: 91–97, 1994. doi:10.1113/jphysiol.1994.sp020343.
 38. **Ward SM, Harney SC, Bayguinov JR, McLaren GJ, Sanders KM.** Development of electrical rhythmicity in the murine gastrointestinal tract is specifically encoded in the tunica muscularis. *J Physiol* 505: 241–258, 1997. doi:10.1111/j.1469-7793.1997.241bc.x.
 39. **Yamazawa T, Iino M.** Simultaneous imaging of Ca2+ signals in interstitial cells of Cajal and longitudinal smooth muscle cells during rhythmic activity in mouse ileum. *J Physiol* 538: 823–835, 2002. doi:10.1113/jphysiol.2001.013045.

